Physica B 528 (2018) 1–8

Contents lists available at ScienceDirect

Physica B

journal homepage: www.elsevier.com/locate/physb

Electronic, magnetic and transport properties of transition metal-doped holely C_2N-*h*2D nanoribbons

Jing-Jing He[a,b], Yan-Dong Guo[a,b,*], Xiao-Hong Yan[a,b,c,d,*], Hong-Li Zeng[a,b]

[a] College of Electronic Science and Engineering, Nanjing University of Posts and Telecommunications, Nanjing 210046, China
[b] Key Laboratory of Radio Frequency and Micro-Nano Electronics of Jiangsu Province, Nanjing 210023, Jiangsu, China
[c] College of Science, Nanjing University of Aeronautics and Astronautics, Nanjing 210016, China
[d] School of Material Science and Engineering, Jiangsu University, Zhenjiang 212013, China

ARTICLE INFO

Keywords:
C_2N-*h*2D nanoribbon
Transition metal doping
Electronic properties
First-principles

ABSTRACT

A novel layered two-dimensional graphene-like material C_2N-*h*2D with evenly distributed holes and nitrogen atoms has been synthesized via a bottom-up wet-chemical reaction [*Nat. Commun.* 6, 6486 (2015)]. The presence of holes provides a ground for further functionalization by doping. By performing a first-principles study, we have doped transition metals at the center of the holes of C_2N-*h*2D nanoribbons and explored their doping effects on electronic, magnetic and transport properties. It is found that the doping can essentially regulate the electronic properties of C_2N-*h*2D nanoribbons. The metallic zigzag ribbon is tuned into a semiconductor for Mn, Fe and Co-doped cases, but half-metal for Ni-doping. This transition is derived from the peculiar band morphology which has a big band gap between the edge state and the higher band, so when the energy of the edge state is reduced by the impurity state, the band gap falls too and crosses the Fermi level. In contrast, the pristine semiconducting armchair C_2N-*h*2D nanoribbon is changed into metallic. Different from the zigzag case, its physical mechanism originates from the hybridization of 3*d* orbitals of transition metal atoms and the *p* orbitals of carbon and nitrogen atoms which introduces several resonant peaks at the Fermi level in the density of states. Furthermore, the magnetic moments of all doped materials are enhanced compared to the pristine structures but decrease as the atomic number of the transition metal atom increases. And the spin polarization of armchair C_2N-*h*2D nanoribbon is increased, while that of the zigzag structure is decreased except the Ni-doped one which is completely spin-polarized suggesting great prospects in the future of spintronics and nanoelectronics.

1. Introduction

The successful experimental preparation with near atomic precision has made the graphene nanoribbon (GNR) into a research hotspot with more attention due to its potential for electronic and spintronic applications [1–3]. The structures and electronic properties of GNRs are determined by their width and the direction-dependent configuration of atoms along their edges [4]. The electronic properties of GNRs can also be monitored via the edge saturation, doping or adsorption by external atoms or molecules [5–15,16,17]. Many efforts are devoted to studying the effect of transition metal (TM) doping or adsorption on the properties of GNRs [4,9,18–22]. For example, Sevin et al. [19] presented whether the armchair graphene nanoribbon (AGNR) was a metal or a semiconductor with ferromagnetic or antiferromagnetic depended on the ribbon width and adsorbed TM atom species. Fe or Ti adsorption made AGNR a half-metal with a 100% spin polarization at the Fermi level. As for zigzag graphene nanoribbon (ZGNR), the electronic character depended on the species and concentration of the adsorbate and on the adsorption site(s), different stable or near-stable systems exhibiting semiconducting, zero-gap semiconducting, metallic, or half-metallic behavior for one or two adatoms of 3*d*, 4*d*, and 5*d* TM [20]. For a single adsorbed Ni atom, the adsorption process reduced the magnetic moment of Ni adatom due to hybridization between the Ni 3*d* orbitals and carbon 2*p* orbitals, and many Ni *d*-related states near the Fermi energy gave rise to a spin-dependent charge transport [9]. Gorjizadeh et al. [21] reported that the AGNRs and ZGNRs doped with 3*d* TMs have a similar spin polarization. In the case of multiple adsorbed atoms, e.g., Ni_4 and Fe_4 nanostructures, both Ni and Fe atoms were most strongly bound at edge sites and neither altered whether the ZGNR was metallic or semiconducting. However, Ni_n nanostructures were more strongly bound than Fe_n nanostructures, and their atoms had much smaller spin magnetic moments [4].

* Corresponding authors at: College of Electronic Science and Engineering, Nanjing University of Posts and Telecommunications, Nanjing 210046, China.
E-mail addresses: yandongguo@njupt.edu.cn (Y.-D. Guo), yanxh@njupt.edu.cn (X.-H. Yan).

http://dx.doi.org/10.1016/j.physb.2017.09.124
Received 5 July 2017; Received in revised form 24 September 2017; Accepted 27 September 2017
Available online 28 September 2017

Recently, a new type of two-dimensional material C_2N-*h*2D synthesized by simple chemical methods has received much attention [23–29]. The graphene-like C_2N-*h*2D material owns evenly distributed nitrogen atoms and holes where the benzene rings are bridged by pyrazine rings with two nitrogen atoms facing each other [25]. Compared to graphene, its band opens a direct gap of 1.70 eV, and the flat bands near the Fermi level are derived from the *p* orbitals of nitrogen atoms. In addition, the presence of holes makes C_2N-*h*2D easier to cocoon some metal particles showing preeminent properties. Mahmood et al. [26] synthesized a two-dimensional (2D) polymer-encapsulated cobalt-oxide catalyst (Co@C2N) which possessed highly active sites and exhibited outstanding catalytic activities towards $NaBH_4$ hydrolysis compared to other metal catalysts. Theoretically, the hole doping could also induce tunable ferromagnetic properties of the 2D C_2N, which was tightly correlated with the localized σ-states of nitrogen atom [27]. Motivated by these experimental and theoretical researches, we dope the TM atoms in the hole center of C_2N-*h*2D nanoribbon (C_2NNR) and focus on the electronic, magnetic and transport properties in the ferromagnetic state. Interestingly, after doping, zigzag C_2N-*h*2D nanoribbons (ZC_2NNRs) change from metallic to semiconducting, except Ni-doped one which shows half-metallic. On the contrary, armchair C_2N-*h*2D nanoribbons (AC_2NNRs) are tuned from original semiconducting to metallic. The magnetic moments of all the nanoribbons become larger and decrease with the increase of the TM atomic number. We also explore the transport properties of the C $_2$ NNRs and find that, after doping, the spin polarizations of AC $_2$ NNRs are increased, among them Ni-doped structure has the maximum of 57%. However the doped ZC $_2$ NNRs have zero spin polarization due to their semiconducting properties, except the half-metallic Ni-doped one which has a 100% spin polarization and can be used as a spin-filter [30].

2. Computational method

The calculations are performed by the Atomistix Toolkit (ATK) package, which is based on the combination of density functional theory (DFT) and non-equilibrium Green's function (NEGF) technique is performed [31]. The mesh cutoff energy is set to be 150 Ry, and the *k*-point mesh is 1 × 1 × 100 in the Monkhorst-Park scheme [32]. The Perdew-Burke-Eenzerhof formulation of the spin generalized gradient approximation (SGGA) is used as the exchange-correlation function, and the double-zeta polarized basis set is employed in the calculations. The vacuum spaces of supercell are set to be more than 15 Å to eliminate the interactions with adjacent images. All the atomic positions of the structure have been optimized until all the forces are smaller than 0.02 eV/Å. The edges of C_2NNRs are terminated with hydrogen (H) atoms to remove the dangling bonds.

3. Results and discussions

As C_2N-*h*2D structure contains holes and nitrogen atoms in addition to carbon atoms, so there are more situations to be cut into a nanoribbon compared to graphene. In this paper, the armchair and zigzag C_2NNRs with carbon atoms as edge atoms are adopted which are depicted in Fig. 1(a) and (b) respectively. Clearly, both armchair and zigzag C_2NNRs have a hole in the center. Fig. 1(c) and (d) show the band structures of the pristine armchair and zigzag C_2NNRs in different magnetic states. For pristine AC_2NNR, spin-polarized calculations with both ferromagnetic (FM) and antiferromagnetic (AFM) initial guess converge to the nonmagnetic (NM) state [30]. Its energy band opens a gap of 0.35 eV at the Γ-point. For pristine ZC_2NNR, the ground state is AFM, and the highest is NM. In the case of NM, there are only two bands in the energy range of [−0.65–1.22] eV which cross each other at the Fermi level. In FM case, the spin-up and spin-down bands maintain a similar shape, but the spin-up bands move up and spin-down bands move down compared to NM's. So only one of their two crossed bands crosses the Fermi level. AFM case is not the same as the previous two cases, spin-up and spin-down bands are degenerated and open a gap of 0.63 eV around the Fermi level, showing semiconductivity which is similar to ZGNR [33,34]. Interestingly, a particular property of the band structure has existed in all three cases, that is, there is a large gap between the band near the Fermi level and the higher band (e.g., shown as the orange line in Fig. 1(d)). We argue that this band feature will have a certain effect on the doping effect. In the following study, we focus on the FM state which can be stabilized by applying a magnetic field [35].

3.1. TM-doped ZC_2NNRs

Fig. 2 shows the doped configurations of ZC_2NNR where TM atoms lie in the central region of the primitive cell, we also try to put the TMs at other sites and calculate their total energies, and find that the one shown in Fig. 2 has the lowest value, so it is the most stable structure. Obviously, after doping, the structures of ZC_2NNRs are bent toward the center due to the bonding of the TM atoms and the nearby N atoms. The bond lengths between Mn, Fe, Co, Ni and nitrogen atoms gradually increase in the range of [1.83, 1.93] Å indicating a decrease of the bond [36]. The binding energies are also calculated as $E_b = E[ZC_2NNR] + E[TM] - E[ZC_2NNR + TM]$ in terms of the total energies of the pristine ZC_2NNR ($E[ZC_2NNR]$), the isolated TM atom ($E[TM]$), and one TM atom doped in ZC_2NNR ($E[ZC_2NNR + TM]$) [19]. The binding energies of Mn, Fe, Co and Ni-doped ZC_2NNRs are 5.16, 6.00, 6.52 and 6.86 eV respectively exhibiting strong binding. Therefore, all TM-doped C2NNRs have good stability.

The projected density of states (PDOS) for TM-doped ZC_2NNRs are presented in Fig. 3. It can be seen that 3*d* orbitals of all TM atoms do not contribute to the spin-up state density and a energy band gap of about 0.8 eV occurs in all doped structures. However for spin-down state density, the 3*d* orbitals of all TM atoms hybridize with the *p* orbitals of the carbon and nitrogen atoms in ZC_2NNR. The energy band gap at the Fermi level is opened and decreases as the dopant TM atomicity increases until it becomes zero due to the presence of the spin-down 3*d* peaks of Ni atom around the Fermi level. So Mn, Fe and Co doped ZC_2NNRs are semiconductors, while Ni doped is a half-metal.

In Fig. 1, we have mentioned that the pristine ZC_2NNR is metallic in the FM state, and the PDOS analysis shows the electronic structure undergoes a great change after the TM atoms are doped. For a better analysis, the band structures of the TM-doped and pristine ZC_2NNRs are plotted in Fig. 4(a) and (b) respectively. For pristine ZC_2NNR, the two crossed spin-up bands at the Fermi level are denoted by n = 1 and 2, respectively. Similarly, the crossed spin-down bands are denoted by n = 1′ and 2′. As previously described, a large gap exists between n = 1 (or n = 1′) and the higher bands. In Fig. 4(c), we plot the distribution of the real-space wave functions of n = 1, 2, 1′ and 2′ bands. Obviously, these four wave functions are mainly distributed on the edge of the nanoribbons, belonging to the edge states. After doping, the two spin-up crossed bands still exist and maintain the original morphology, but their energies are reduced as depicted in Fig. 4(a). We choose the Fe-doped structure as a representative to show the wave functions of the spin-up n = 1 and 2 bands in Fig. 4(d). It is clear that the doping of the transition metal atoms does not destroy the edge state. Interestingly, due to the decline in energy, the original energy gap also moves down and cross the Fermi level, so the spin-up bands of four TM-doped materials show the nature of the semiconductor. In addition, we should note that for these four dopant atoms, the degree of energy reduction in the spin-up energy level is getting smaller and smaller and becomes minimal for Ni doped structure.

For the spin-down bands, we give out the real space distribution of the non-local two bands near the Fermi level and denote them with n = 3′ and 4′ in Fig. 4(e). For the Mn-doped structure, it is obvious that the wave functions of n = 3′ and 4′ are localized at the edge of the

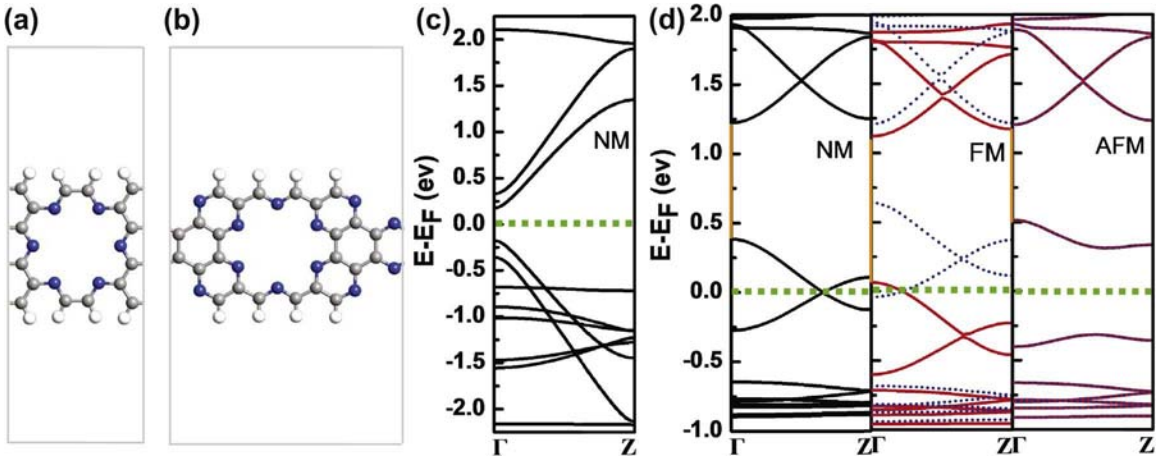

Fig. 1. Schematic illustration of (a) pristine AC_2NNR; (b) pristine ZC_2NNR. Nitrogen, carbon and hydrogen atoms are shown by blue, gray and white balls, respectively. Band structures around the Fermi level of (c) nonmagnetic (NM) AC_2NNR; (d) nonmagnetic, ferromagnetic (FM) and antiferromagnetic (AFM) ZC_2NNRs. The red solid line represents spin-up bands, blue dotted line denotes spin-down bands and the green dotted line is the Fermi level. (For interpretation of the references to color in this figure legend, the reader is referred to the web version of this article.)

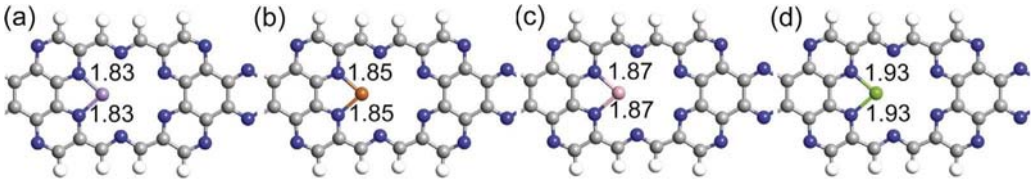

Fig. 2. Schematic illustration of (a) Mn-doped; (b) Fe-doped; (c) Co-doped; (d) Ni-doped ZC_2NNR. The unit cell is omitted, the same as below. Nitrogen, carbon and hydrogen atoms are shown by blue, gray and white balls, respectively. The bond lengths of the transition metals and nitrogen atoms are marked in units of Å. (For interpretation of the references to color in this figure legend, the reader is referred to the web version of this article.)

nanoribbons belonging to edge state. Both their energies are reduced compared to those of the pristine ZC_2NNR and open a band gap of 0.72 eV. For Fe-doped structure, from the wave function of n = 3′, one finds that the contribution of the *d*-orbital of the Fe atom is distinct. However the wave function distribution of n = 4′ is the same as that of Mn doping case, belonging to the edge state, but its energy is higher. The band gap is 0.47 eV between n = 3′ and n = 4′. For Co doping case, the wave functions of n = 3′ and n = 4′ are derived from the joint contribution between the edge atom and the *d* orbital of Co atom. The energy of n = 4′ is significantly increased relative to the first two dopants, so the band gap is reduced to 0.15 eV. For the Ni-doped structure, the wave function of n = 3′ is more delocalized than the previous three kinds of doping, and the contribution of *d* orbital of the Ni atom is more prominent in the wave function of n = 4′. So the

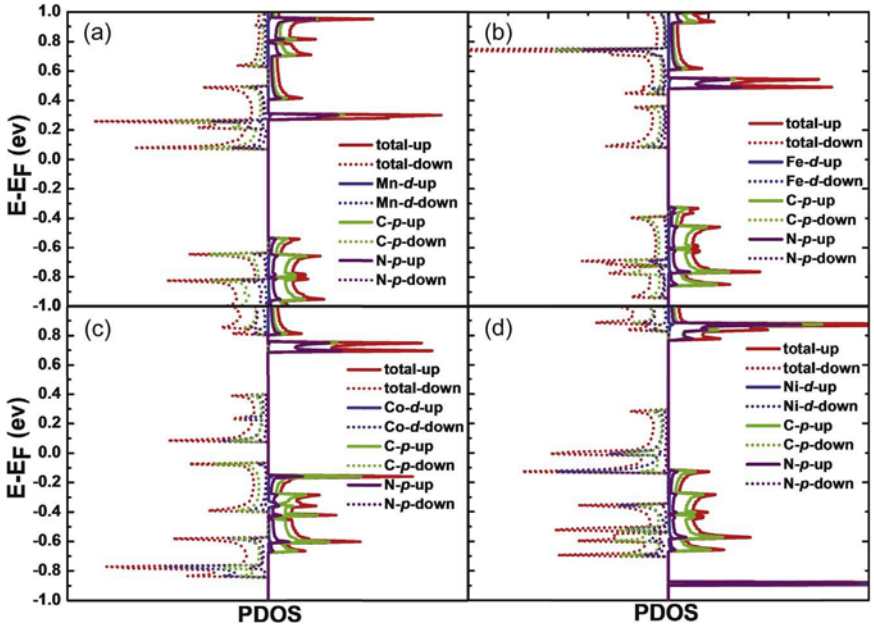

Fig. 3. PDOSs of (a) Mn-doped; (b) Fe-doped; (c) Co-doped; (d) Ni-doped zigzag C_2N-*h*2D nanoribbon; The solid line represents spin-up bands, dotted line denotes spin-down bands and red, blue, green, purple lines denote total, *d* orbital of TM atoms, *p* orbital of carbon atom and *p* orbital of nitrogen atom respectively. (For interpretation of the references to color in this figure legend, the reader is referred to the web version of this article.)

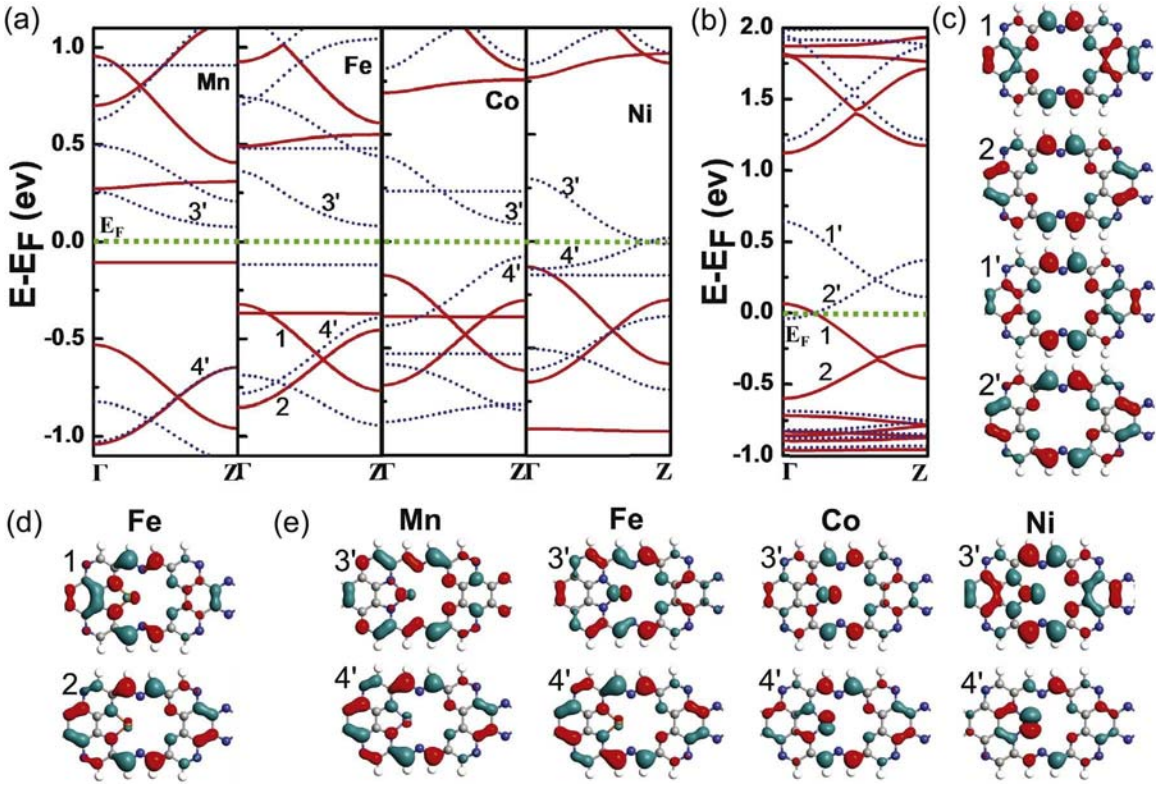

Fig. 4. (a) Band structure around the Fermi level of Mn, Fe, Co and Ni-doped ZC_2NNR; The red solid line represents spin-up bands, blue dotted line denotes spin-down bands and the green dotted line is the Fermi level. (b) Band structure around the Fermi level of ferromagnetic pristine ZC_2NNR. (c) Isosurface plots of the Γ-point wave functions of n = 1,2 and n = 1′,2′ subbands of pristine ZC_2NNR. (d) Isosurface plots of the Γ-point wave functions of n = 1,2 subbands of Fe-doped ZC_2NNR. (e)Isosurface plots of the Γ-point wave functions of n = 3′,4′ subbands of Mn, Fe, Co and Ni-doped ZC_2NNR. (For interpretation of the references to color in this figure legend, the reader is referred to the web version of this article.)

contributions of the dopant atoms in the two nonlocal spin-down bands near the Fermi level is more and more pronounced and the two bands are getting closer and closer until finally cross each other at the Fermi level, hence the Ni-doped ZC_2NNR becomes a half-metal.

In general, after doping TMs, the energies of the bands near the Fermi level decrease compared to the pristine ZC_2NNR, and the differences reduce with the increase of TM atomic number. This may result from the interaction between the TM atom and the nanoribbon, while this effect is impaired as the increase of the bond length between the TM atom and the ZC_2NNR (as shown in Fig. 2), so as the atomic number of TM atom increases, the magnitude of the energy reduction becomes smaller [37,38].

We also explore the magnetic properties of the ZC_2NNR and find that the magnetic moment of the pristine structure is 1.6 μ_B. For an isolated Mn, Fe, Co and Ni atom, the ground-state configuration is 4 $s^2 3d^5$, 4 $s^2 3d^6$, 4 $s^2 3d^7$ and 4 $s^2 3d^8$ respectively. After Mn, Fe, Co and Ni-doping, the magnetic moments of the materials are respectively 5.0, 4.0, 3.0 and 2.0 μ_B. Magnetic moments decrease with increasing atomic number which is because the number of unpaired electrons of 3*d* orbitals decreases with increasing atomic number [21].

Fig. 5 shows the electron transmission spectra of the ZC_2NNRs after doping TM atoms. Since the Mn, Fe and Co-doped structures are semiconducting, the transport coefficients are all zero at the Fermi level. However, if the energy is slightly higher, it can be seen that the spin-down has a transmission peak and the spin-up transport coefficient is zero. We here define the spin polarization as (up-down)/(up+down)×100%. So the spin polarization will be −100%. Therefore, the spin polarization can be increased at the Fermi level by applying a gate voltage or other regulatory methods [39]. For the Ni-doped structure, the semi-metallic property is present. The spin-up transport coefficient at the Fermi level is zero but that of spin-down is 0.8 indicating a spin polarization of −100%. So Ni-doped structure can be applied to the spin filter device, which has a good application prospect in nanoelectronics.

3.2. TM-doped AC_2NNRs

Fig. 6(a) shows a schematic representation of the TM-doped AC_2NNRs. Similar to the zigzag type, the structures are slightly bent toward the center due to the bonding of the metal atoms to the surrounding nitrogen atoms. For Mn, Fe and Co atoms, the bonds between TM and N atoms are divided into two types, with bond lengths of 2.06 and 1.76 Å, respectively. However Ni-N bonds have larger lengths of 2.15 and 1.86 Å respectively, indicating weaker bondings [36]. The binding energies of Mn,Fe, Co and Ni-doped AC_2NNRs are 4.78, 5.65, 6.28 and 6.74 eV respectively which are lower that those of doped ZC_2NNRs but still shows strong binding.

The PDOS for TM-doped AC_2NNR is presented in Fig. 7. Different from the case of TM-doped ZC_2NNR, all TM-doped AC_2NNRs exhibit metallic due to the occurrence of spin-up and down peaks at the Fermi level. In addition, for the spin-up case, the contribution of the 3*d* orbitals of Mn and Co at the Fermi level is significant having a large degree of hybridization with the *p*-orbitals of the carbon and nitrogen atoms of the nanoribbons. While the contribution of Fe 3*d* orbitals is almost nonexistent, and the hybrid peak of the Ni 3*d* orbitals and C and N *p*-orbitals is relatively small. In the case of spin-down, for Mn, Fe and Co doping, the contributions of the 3*d* orbitals are very noticeable, however the contributions of the Ni 3*d* orbitals is almost zero until the energy down to −0.8 eV below the Fermi level.

For a more detailed analysis, we plot the band structures of TM-doped AC_2NNR in Fig. 8(a). As predicted by the PDOS, for all the doped structures, both spin-up and spin-down bands cross the Fermi level, which tunes the semiconductivity of pristine AC_2NNR nanoribbon into metallicity. For Mn and Co doping cases, spin-up conducting channels are three, while two and one for Fe and Ni doping respectively. The number of spin-down conducting channels is one for Mn and Fe doped structures, while two for Co and Ni cases. In order to

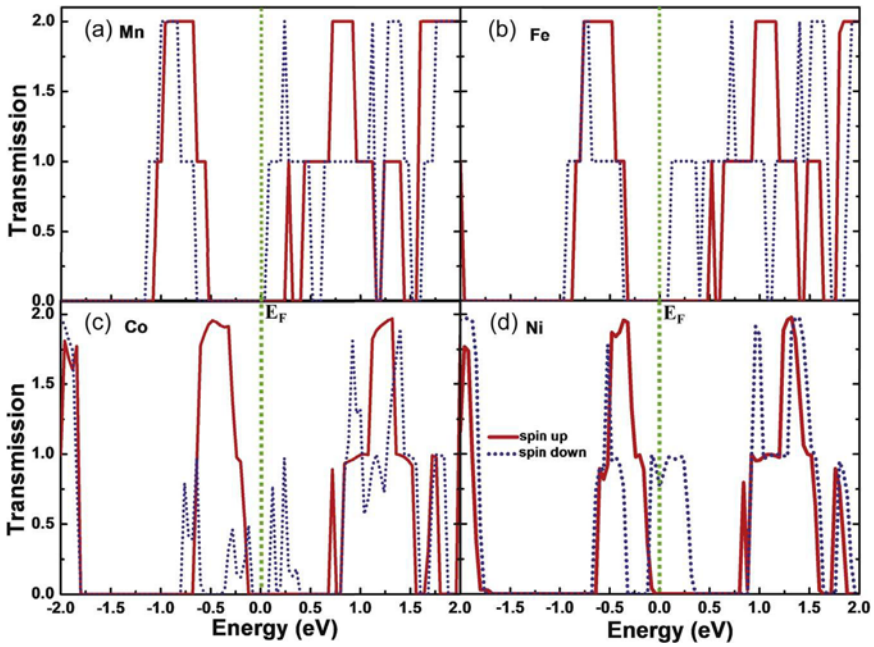

Fig. 5. The transmission spectra of (a) Mn-doped; (b) Fe-doped; (c) Co-doped; (d) Ni-doped ZC_2NNR under bias of V_b = 0 V. Zero energy is the Fermi level.

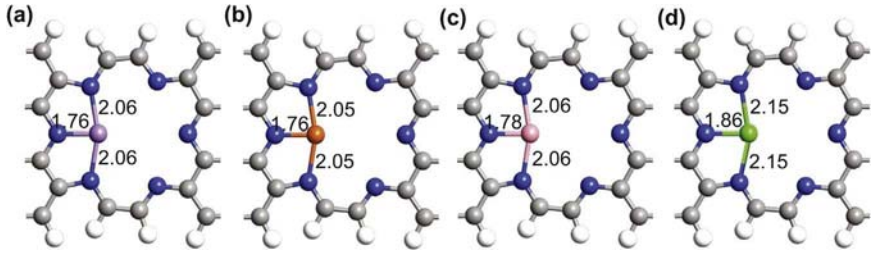

Fig. 6. Schematic illustration of (a) Mn-doped; (b) Fe-doped; (c) Co-doped; (d) Ni-doped AC_2NNR. Nitrogen, carbon and hydrogen atoms are shown by blue, gray and white balls, respectively. The bond lengths of the transition metals and nitrogen atoms are marked in units of Å.

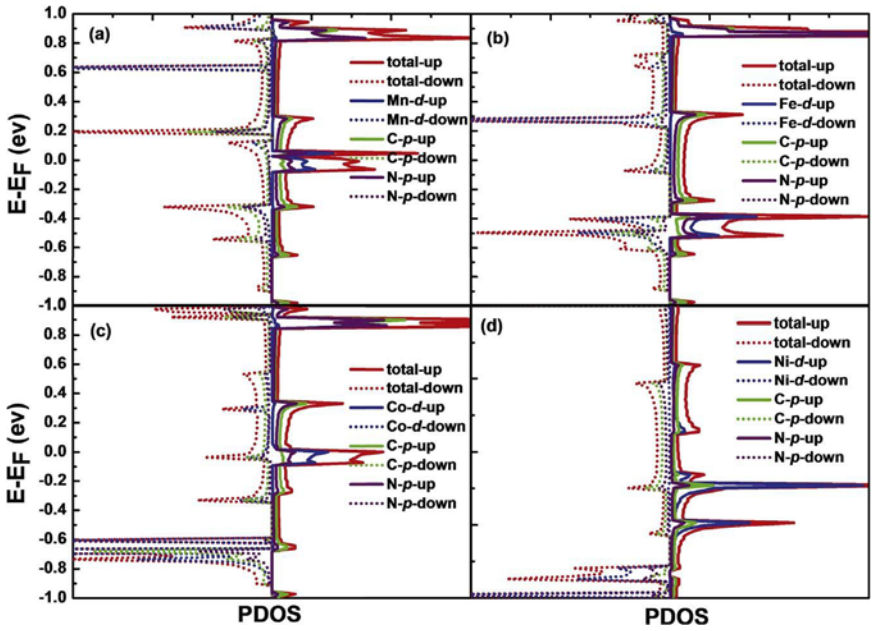

Fig. 7. PDOSs of (a) Mn-doped; (b) Fe-doped; (c) Co-doped; (d) Ni-doped AC_2NNR; The solid line represents spin-up bands, dotted line denotes spin-down bands and red, blue, green, purple lines denote total, *d* orbital of TM atoms, *p* orbital of carbon atom and *p* orbital of nitrogen atom respectively. (For interpretation of the references to color in this figure legend, the reader is referred to the web version of this article.)

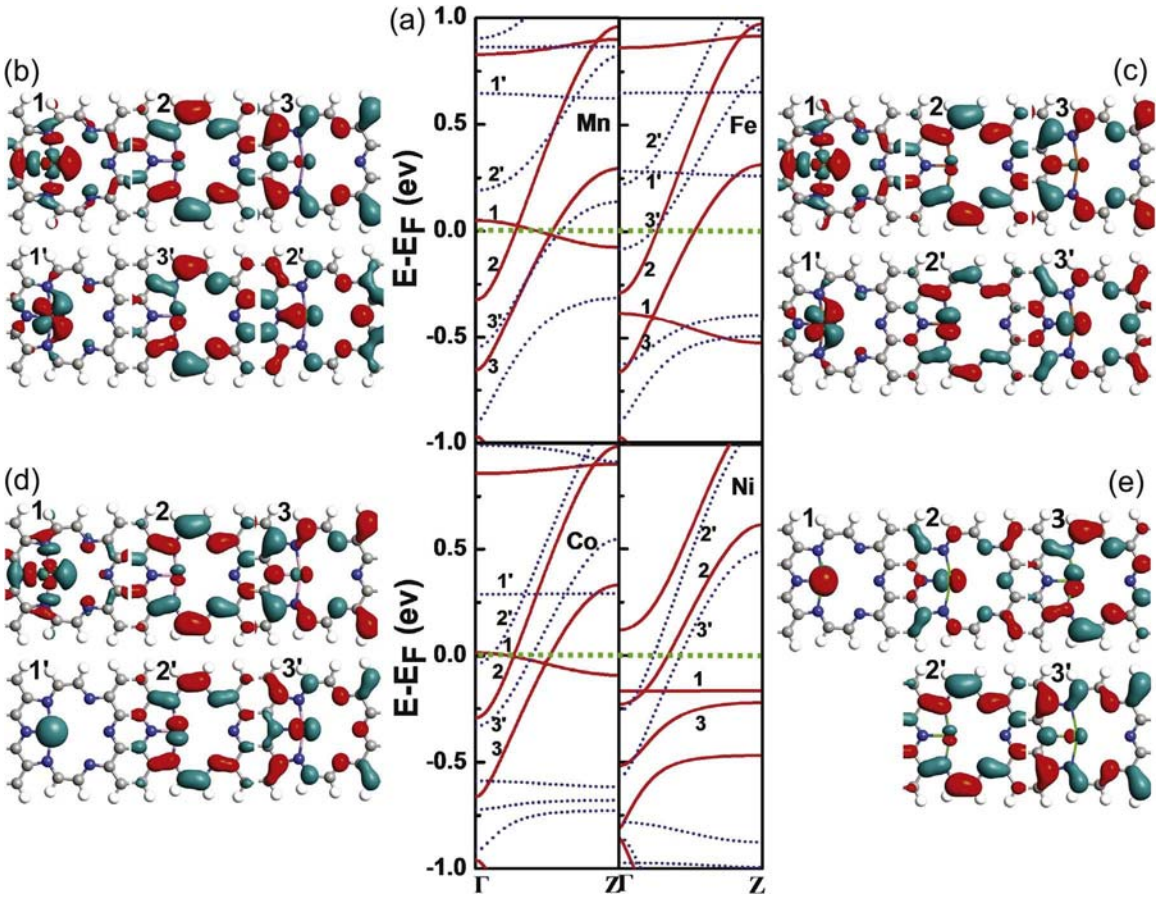

Fig. 8. (a) Band structure around the Fermi level of Mn, Fe, Co and Ni-doped AC_2NNR; The red solid line represents spin-up bands, blue dotted line denotes spin-down bands and the green dotted line is the Fermi level. Isosurface plots of the Γ-point wave functions of n = 1,2,3,4 and n = 1′,2′,3′,4′ subbands of (b) Mn-doped; (c) Fe-doped; (d) Co-doped; (e) Ni-doped AC_2NNR. (For interpretation of the references to color in this figure legend, the reader is referred to the web version of this article.)

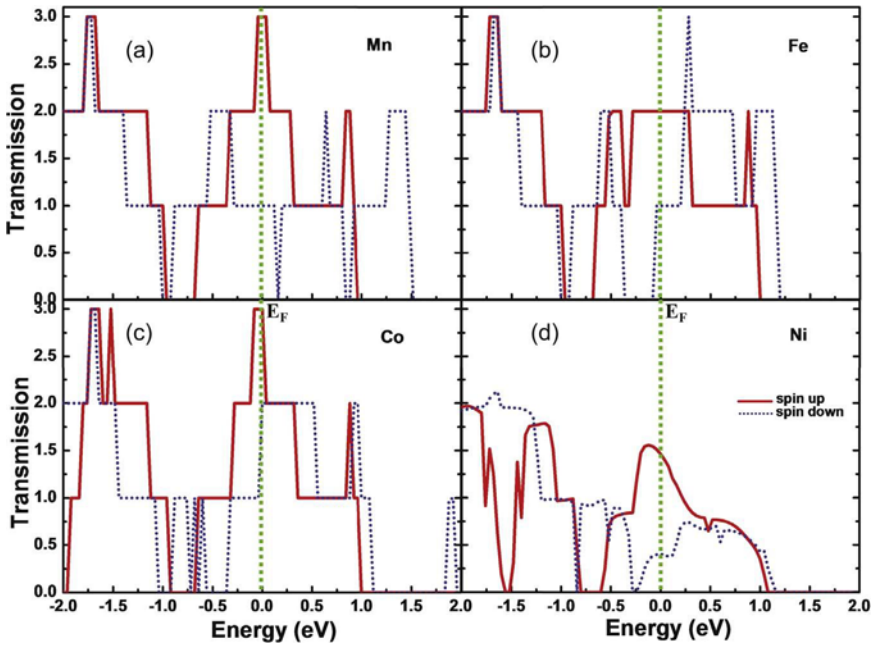

Fig. 9. The transmission spectra of (a) Mn-doped; (b) Fe-doped; (c) Co-doped; (d) Ni-doped AC_2NNR under bias V_b = 0 V. Zero energy is the Fermi level.

understand the contribution of the atomic orbital more intuitively, we draw the wave function of the real space of the spin-up and down bands near the Fermi level as shown in Fig. 8. The red solid line represents the spin up, the three lines are marked as n = 1, 2, 3, and the blue dashed line represents the spin-down, followed by n = 1′, 2′, 3′.

It is not difficult to see that for Mn, Fe and Co doped structures, the wave functions of three spin-up bands are the same. The wave function of n = 1 is localized around the transition metal atom, corresponding to

the d_{xy} orbital, while the wave functions of n = 2 and 3 mainly derive from the p_z orbitals of carbon and nitrogen atoms, and the contribution of metal atoms is very small. For the spin-down bands, the wave function of n = 1′ is localized at the metal atom, corresponding to $d_{x^2-y^2}$ orbital of Mn and Fe and the d_{z^2} orbital of Co, respectively. For n = 2′ and 3′ bands, the distribution of the wave function of these three structures is consistent with the contribution of d_{yz} and d_{xz} orbitals of the metal atoms and the p_z orbitals of the carbon and nitrogen atoms respectively. For Ni-doped structure, the distribution of wave functions is not the same. All the wave functions of the spin-up bands have the contribution of the d orbitals of Ni, where the wave function of the n = 1 band originates from the Ni's d_{z^2} orbital, and the wave functions of n = 2 and 3 bands derive from Ni's d_{xz}, d_{yz} with the p_z orbitals of the carbon and nitrogen atoms. However for the spin-down bands, Ni atoms contribute very little. Because of the difference in the energy and the hybridization of the dopant atoms, the energies of the three bands near the Fermi level are different. So the number of bands that cross the Fermi level is not the same, but the overall structure shows metallic. We also calculated the magnetic moments of the materials. For Mn, Fe, Co and Ni doping, the magnetic moments of material are respectively 3.8, 3.6, 2.0 and −1.3 μ_B. Consistent with the TM-doped ZC_2NNR, the magnetic moment decreases with increasing atomic number of dopant atoms.

In order to further verify the electron transport properties of the two-probe systems composed by TM-doped AC_2NNRs, we calculated their transmission spectra under bias V_b = 0 V. As can be seen from Fig. 9, at the Fermi level, both the spin-up and down transmission coefficients are nonzero. This is due to the presence of spin-up and down bands crossing the Fermi level (shown in Fig. 8(a)). So there are conductive channels and the electrons can be transmitted indicating metallic properties. In addition, the transmission spectra of Mn, Fe, Co-doped structure show jagged, while Ni-doped material transmission spectrum shows wavy. The spin polarizations of these four structures at the Fermi level are found to be 50%, 33%, 20% and 57%, respectively. Interestingly, like ZC_2NNR, the Ni-doped structure has the largest spin polarization, showing a good application prospect in nanoelectronics.

In the above calculations, we use the GGA method to simulate the property of the C_2NNR. Due to the presence of 3d electrons, we also examine the effect of GGA + U on the electronic properties [40,41]. Following several other studies of the TM-containing structures, we set the value of U to 4.0 eV [41–43]. As a result, the addition of U has no fundamental effect on the electronic properties of other structures, only Ni-doped ZC_2NNR is modulated from half-metal into metal. We further test the electronic properties of Ni-doped ZC_2NNR with U values of 0.5, 1.0, 2.0 and 6.0 eV. When U is less than 2.0 eV, we obtain the same conclusion as the case without adding U. When U is greater than or equal to 2.0 eV, the other properties remain unchanged, only Ni-doped ZC_2NNR becomes a metal due to a slight increase in the energy of the spin-up valence band maximum, which allows this band to cross the Fermi level.

4. Conclusion

In conclusion, we have studied the electronic, magnetic and transport properties of TM-doped zigzag and armchair C_2NNRs using a first principles method. The presence of these impurities changes the electronic properties of the nanoribbons. In the ferromagnetic state, the ZC_2NNRs change from the original metals to semiconductors, except the Ni-doped one showing half-metallic. AC_2NNRs are changed from the original semiconductors into metals. The physical mechanisms of these two changes are not the same. For the former, the impurity state does not change the shape of the spin-up electronic structure but results in a energy decrease in the edge state, so the large energy band gap which exists in the pristine nanoribbon crosses the Fermi level showing semiconducting. In the case of spin down, the doping makes the crossed energy bands at the Fermi level be separated from each other, and the energy of valence band maximum for the Mn doping is reduced significantly. Later, due to the more and more larger contribution of the 3d orbitals of TM atoms, the gap between the two separated band is getting smaller and smaller, and finally becomes zero for Ni-doped structure presenting half-metallic property. For the armchair structures, the hybridization of 3d orbitals of TM atoms and p orbitals of carbon and nitrogen atoms introduces several resonance peaks at Fermi level in DOS, so both the spin-up and spin-down have conductive channels showing metallic. The magnetic properties of all the materials are enhanced after the doping, and the magnetic moment decreases with the increase of the atomic number of the transition metal atoms owing to the decreasing number of free electrons. As a result of the changes of electronic structures, after doping with TM, the electron spin polarization of AC_2NNR is increased and the maximum spin polarization at Fermi level is 57%. However the spin polarization of the ZC_2NNR is decreased, except Ni doped structure which has a spin polarization of 100% suggesting a great prospect in the future of spin electronics and nanoelectronics. If the method of GGA + U is used to calculate, when U is less than 2, we can obtain the same conclusion, and when U is greater than or equal to 2, only Ni-doped ZC_2NNR is converted from half-metal to metal due to the increasing energy of the spin-up band near the Fermi level.

Acknowledgement

This work is supported by the National Natural Science Foundation of China (NSFC11504178, NSFC11374162, NSFC11247033 and NSFC51651202), the Natural Science Foundation of Jiangsu Province (BK20150825 and TJ215009), the Scientific Research Foundation of Nanjing University of Posts and Telecommunications (NY214010 and NY217013), and the Fundamental Research Funds for the Central Universities (NS2014073).

References

[1] X. Li, X. Wang, L. Zhang, S. Lee, H. Dai, Chemically derived, ultrasmooth graphene nanoribbon semiconductors, Science 319 (5867) (2008) 1229–1232.
[2] M. Topsakal, H. Sevinçli, S. Ciraci, Spin confinement in the superlattices of graphene ribbons, Appl. Phys. Lett. 92 (17) (2008) 666.
[3] A. Saffarzadeh, R. Farghadan, A spin-filter device based on armchair graphene nanoribbons, Appl. Phys. Lett. 98 (2) (2011) 204.
[4] R.C. Longo, J. Carrete, J. Ferrer, L.J. Gallego, Structural, magnetic, and electronic properties of nin and fen nanostructures ((n=1-4)) adsorbed on zigzag graphene nanoribbons, Phys. Rev. B 81 (11) (2010) 115418.
[5] D. Soriano, F. Muñoz-Rojas, J. Fernández-Rossier, J.J. Palacios, Hydrogenated graphene nanoribbons for spintronics, Physical Rev. B Condens. Matter 81 (16) (2010) 2149.
[6] F. Cervantes-Sodi, G. Cs Aacute, nyi, S. Piscanec, A. C. Ferrari, Edge-functionalized and substitutionally doped graphene nanoribbons: Electronic and spin properties, Physical Review B Condensed Matter 77 (16) (2007) 165427.
[7] Y. Li, Z. Zhou, P. Shen, Z. Chen, Spin gapless semiconductor-metal-half-metal properties in nitrogen-doped zigzag graphene nanoribbons, ACS Nano 3 (7) (2009) 1952–1958.
[8] Y. Wang, C. Cao, H.P. Cheng, Metal-terminated graphene nanoribbons, Phys. Rev. B Condens. Matter 82 (20) (2010) 2889–2898.
[9] V.A. Rigo, T.B. Martins, A.J.R.D. Silva, A. Fazzio, R.H. Miwa, Electronic, structural, and transport properties of ni-doped graphene nanoribbons, Phys. Rev. B Condens. Matter 79 (7) (2009) 075435.
[10] D.E. Jiang, B.G. Sumpter, S. Dai, Unique chemical reactivity of a graphene nanoribbon's zigzag edge, J. Chem. Phys. 126 (13) (2007) 134701.
[11] O. Hod, V. Barone, J.E. Peralta, G.E. Scuseria, Enhanced half-metallicity in edge-oxidized zigzag graphene nanoribbons, Nano Lett. 7 (8) (2007) 2295–2299.
[12] D. Gunlycke, J. Li, J.W. Mintmire, C.T. White, Altering low-bias transport in, Appl. Phys. Lett. 91 (91) (2007) (112108-112108-3).
[13] T.B. Martins, R.H. Miwa, S.A. Da, A. Fazzio, Electronic and transport properties of boron-doped graphene nanoribbons, Phys. Rev. Lett. 98 (19) (2007) (304C308).
[14] B. Huang, Q. Yan, G. Zhou, J. Wu, Making a field effect transistor on a single graphene nanoribbon by selective doping, Appl. Phys. Lett. 91 (25) (2007) (253122-253122-3).
[15] S.S. Yu, W.T. Zheng, Q.B. Wen, Q. Jiang, First principle calculations of the electronic properties of nitrogen-doped carbon nanoribbons with zigzag edges, Carbon 46 (3) (2008) 537–543.
[16] H. Zheng, W. Duley, Field effects on the electronic and spin properties of undoped and doped graphene nanodots, Phys. Rev. B 78 (15) (2008) 155118.
[17] G. Giovannetti, Doping graphene with metal contacts, Phys. Rev. Lett. 101 (2)

(2008) 026803.
[18] S. Kattel, Magnetic properties of 3d transition metals and nitrogen functionalized armchair graphene nanoribbon, RSC Adv. 3 (43) (2013) 21110–21117.
[19] H. Sevinçli, M. Topsakal, E. Durgun, S. Ciraci, Electronic and magnetic properties of 3d transition-metal atom adsorbed graphene and graphene nanoribbons, Phys. Rev. B 77 (19) (2008) 3107–3109.
[20] R.C. Longo, J. Carrete, L.J. Gallego, Ab initio study of 3d, 4d, and 5d transition metal adatoms and dimers adsorbed on hydrogen-passivated zigzag graphene nanoribbons, Phys. Rev. B 83 (23) (2011) 7906.
[21] N. Gorjizadeh, A.A. Farajian, K. Esfarjani, Y. Kawazoe, Spin and band-gap engineering in doped graphene nanoribbons, Phys. Rev. B 78 (15) (2008) 155427.
[22] Y. Wang, H.P. Cheng, Interedge magnetic coupling in transition-metal terminated graphene nanoribbons, Phys. Rev. B 83 (11) (2011) 113402.
[23] J. Mahmood, E.K. Lee, M. Jung, D. Shin, I.-Y. Jeon, S.-M. Jung, H.-J. Choi, J.-M. Seo, S.-Y. Bae, S.-D. Sohn, et al., Nitrogenated holey two-dimensional structures, Nat. Commun. 6 (2015) 1–7.
[24] R. Zhang, B. Li, J. Yang, Effects of stacking order, layer number and external electric field on electronic structures of few-layer c2n-h2d, Nanoscale 7 (33) (2015) 14062.
[25] H. Sahin, Structural and phononic characteristics of nitrogenated holey graphene, Phys. Rev. B 92 (8) (2015) 085421.
[26] J. Mahmood, S.M. Jung, S.J. Kim, J. Park, J.W. Yoo, J.B. Baek, Cobalt oxide encapsulated in c2n-h2d network polymer as a catalyst for hydrogen evolution, Chem. Mater. 27 (13) (2015) 4860–4864.
[27] Z. Liang, B. Xu, H. Xiang, Y. Xia, J. Yin, Z. Liu, Carrier-tunable magnetism in two dimensional graphene-like c2n, RSC Adv. 6 (59) (2016) 54027–54031.
[28] S. Guan, Y. Cheng, C. Liu, J. Han, Y. Lu, S.A. Yang, Y. Yao, Effects of strain on electronic and optic properties of holey two-dimensional c2n crystals, Appl. Phys. Lett. 107 (23) (2015) 666.
[29] Z. Guan, J. Li, W. Duan, Graphene/g-c2n bilayer: gap opening, enhanced visible light response and electrical field tuning band structure, Physics 81 (20) (2015) 2498–2502.
[30] C. Cao, M. Wu, J. Jiang, H.-P. Cheng, Transition metal adatom and dimer adsorbed on graphene: induced magnetization and electronic structures, Phys. Rev. B 81 (20) (2010) 205424.
[31] M. Brandbyge, J.-L. Mozos, P. Ordejón, J. Taylor, K. Stokbro, Density-functional method for nonequilibrium electron transport, Phys. Rev. B 65 (16) (2002) 165401.
[32] H. Monkhorst, J. Pack, Special points for brillouin-zone integrations, Phys. Rev. B 13 (1976) 5188.
[33] Y.W. Son, M.L. Cohen, S.G. Louie, Half-metallic graphene nanoribbons, Nature 444 (7117) (2007) 347.
[34] Y. Sugai, Energy gaps in graphene nanoribbons, Phys. Rev. Lett. 97 (21) (2006) 216803.
[35] F. Muñozrojas, J. Fernndezrossier, J.J. Palacios, Giant magnetoresistance in ultrasmall graphene based devices, Phys. Rev. Lett. 102 (13) (2009) 136810.
[36] A.V. Krasheninnikov, P.O. Lehtinen, A.S. Foster, P. Pyykkö, R.M. Nieminen, Embedding transition-metal atoms in graphene: structure, bonding, and magnetism, Phys. Rev. Lett. 102 (12) (2009) 126807.
[37] Y. Gai, J. Li, S.-S. Li, J.-B. Xia, S.-H. Wei, Design of narrow-gap tio 2: a passivated codoping approach for enhanced photoelectrochemical activity, Phys. Rev. Lett. 102 (3) (2009) 036402.
[38] X. Tan, L. Wang, H. Shao, S. Yue, J. Xu, G. Liu, H. Jiang, J. Jiang, Improving thermoelectric performance of imgagsb by theoretical band engineering design, Adv. Energy Mater. 9 (2017) 036402.
[39] Y.-W. Son, M.L. Cohen, S.G. Louie, Half-metallic graphene nanoribbons, Nature 444 (7117) (2006) 347–349.
[40] Q. Tang, Z. Zhou, Z. Chen, Innovation and discovery of graphene-like materials via density-functional theory computations, Wiley Interdiscip. Rev. Comput. Mol. Sci. 5 (5) (2015) (360C379).
[41] D. Ghosh, G. Periyasamy, B. Pandey, S.K. Pati, Computational studies on magnetism and the optical properties of transition metal embedded graphitic carbon nitride sheets, J. Mater. Chem. C 2 (37) (2014) 7943–7951.
[42] M. Bernien, J. Miguel, C. Weis, M.E. Ali, J. Kurde, B. Krumme, P.M. Panchmatia, B. Sanyal, M. Piantek, P. Srivastava, Tailoring the nature of magnetic coupling of fe-porphyrin molecules to ferromagnetic substrates, Phys. Rev. Lett. 102 (4) (2009) 047202.
[43] J. Zhou, Q. Sun, Magnetism of phthalocyanine-based organometallic single porous sheet, Journal of the Am. Chem. Soc. 133 (38) (2011) 15113–15119.